Functional hyperspectral imaging captures subtle details of cell metabolism in olfactory neurosphere cells, disease –specific models of neuronal disorders

Martin E. Gosnell[1,3], Ayad G. Anwer[1], Juan C. Cassano[2], Carolyn M. Sue[2] and Ewa M. Goldys[1*]

[1]ARC Centre of Excellence in Nanoscale BioPhotonics, Macquarie University, Sydney, 2109, New South Wales, Australia.

[2]Department of Neurogenetics, Kolling Institute, Royal North Shore Hospital/Northern Clinical School, University of Sydney, New South Wales, Australia.

[3] Quantitative Pty Ltd, ABN 17 165 684 186, www.quantitative.net.au, tel. +614 22 498 630

**Corresponding author ewa.goldys@mq.edu.au*

Abstract

Hyperspectral imaging uses spectral and spatial image information for target detection and classification. In this work hyperspectral autofluorescence imaging was applied to olfactory neurosphere-derived cells as a human metabolic disease cell model of MELAS (mitochondrial myopathy, encephalomyopathy, lactic acidosis, stroke-like syndrome). By using endogenous source of contrast we have been able to detect subtle metabolic variations between living cells in their full morphological context and differentiate healthy from diseased cells before and after therapy. Cellular maps of native fluorophores, flavins, bound and free NADH and retinoids unveiled subtle metabolic signatures and helped uncover medically significant cell subpopulations, in particular a subpopulation with simultaneous low bound NADH, high free NADH and high lipofuscin content. Taken together, our results demonstrate that hyperspectral imaging provides a new method to investigate neuronal and other diseases, and it paves the way for novel diagnostics and monitoring of therapies with proper account of intrinsic cellular heterogeneity.

Introduction

Olfactory neurosphere (ONS) cells are easily accessible, patient-derived models of neurological disease [1]. They are harvested from the human olfactory mucosa, the organ of smell in the nose, which regenerates throughout life. This neural tissue is accessible in human adults and it demonstrates disease-dependent cell biology alterations for example in Alzheimer's and Parkinson's disease, Rett syndrome, fragile X syndrome, schizophrenia, MELAS and others [2-8]. The analysis of such cells provides new routes for the understanding the pathogenesis of complex neuronal diseases. As neurons exhibit intense metabolic demands, the impairment of cellular metabolism is frequent in many neurodegenerative diseases. Thus new methods are required to characterise and quantify metabolism on a single cell level. Such methods are important for more accurate early diagnosis, treatment monitoring or the development of therapies, especially that some fragile cells such as, for example motor neurones can not be analysed by conventional methods such as flow cytometry.

Monitoring of endogenous cell fluorophores including nicotinamide adenine dinucleotide (NADH), nicotinamide adenine dinucleotide phosphate (NADPH), flavin adenine dinucleotide (FAD) and flavin mononucleotide (FMD) to investigate cell metabolism has been pioneered by Chance and his group [9]. By using optical microscopy techniques, these compounds can be easily observed

providing insights into metabolic activity in cells without altering them with exogenous labels [10-27]. Multiphoton and fluorescence lifetime imaging microscopy (FLIM) have been the leading methods of cellular autofluorescence imaging with pioneering works by Skala et al. [10-12], Gratton's group [15-20], and others. Multiphoton and FLIM imaging makes it possible to determine the relative amounts of FAD and reduced NADH and to distinguish their free and protein-bound forms. This has been used to document increased glycolysis in cancer cells [10-13]. Although quantitative analysis of autofluorescence has been previously explored in multiphoton and FLIM modalities, there has been no previous in-depth work concerned with single photon excited fluorescence. This simple approach provides clinically important information, and it can be carried out by using unsophisticated, low cost instrumentation.

Here we report the application of hyperspectral autofluorescence analysis to functional, metabolic imaging of olfactory neurosphere-derived cells from patients suffering from mitochondrial disease, commonly attributed to the m.3243A>G mitochondrial DNA (mtDNA) point mutation [28-31]. This mitochondrial disease is referred to as MELAS syndrome and its severity is indicated by the percentage of mutated genes (see Sup. Mat. for more details). It is thought that mutations within the *MT-TL1* gene such as m.3243A>G can disrupt mitochondrial function, impair mitochondrial protein synthesis [28], reduce mitochondrial respiratory chain enzyme activities [29] and ultimately reduce the ATP production [32]. Mitochondrial parameters are subsequently affected, with studies reporting reduced mitochondrial membrane potential, with a parallel increase in reactive oxygen species production leading to reduced ATP production and induction of mitochondrial permeability [29]. Cellular damage is apparent too, with increased glycolytic rate, impaired NADH response, decreased glucose oxidation and increased lactate production [31]. The defective oxidative metabolism, may also influence clinical expression of disease. For example, neurons and myocytes are greatly affected by mtDNA mutations, as they are highly metabolic cells. A further feature of the MELAS syndrome is the phenomenon of 'heteroplasmy', where cells differ in their proportion of mutant versus wild-type mtDNA. Thus the analysis method that is able to yield quantitative insights concerning metabolism of individual live cells as well as their populations is a valuable tool to improve the understanding of this disease. This work shows that a simple hyperspectral imaging system coupled to a conventional wide-field microscope and high content analysis of the images provide novel insights into cell metabolic signatures, their heterogeneity and MELAS disease biology.

Throughout this work, hyperspectral autofluorescence images of live cells have been obtained at a number of excitation wavelength ranges between 334 and 495 nm (each 10 nm wide). The emission is detected in the range 550 nm- 600 nm. See Supplementary Material S1-S4 for a full description of methods.

Results

Hyperspectral imaging can distinguish MELAS patients from healthy controls and confirms the effectiveness of galactose treatment

First we show the results of our characterisation of olfactory neurosphere cells with high and lower mutant loads of the m.3243A>G mutation ("MELAS cells") and control cells. Average cell spectra (represented by single data points) have been plotted in a two-dimensional spectral space produced

by linear discriminant analysis (LDA, see Sup. Mat. S1) to optimally separate the three groups of cells: healthy cells from both controls, 11% mutant MELAS and 44% mutant MELAS cells.

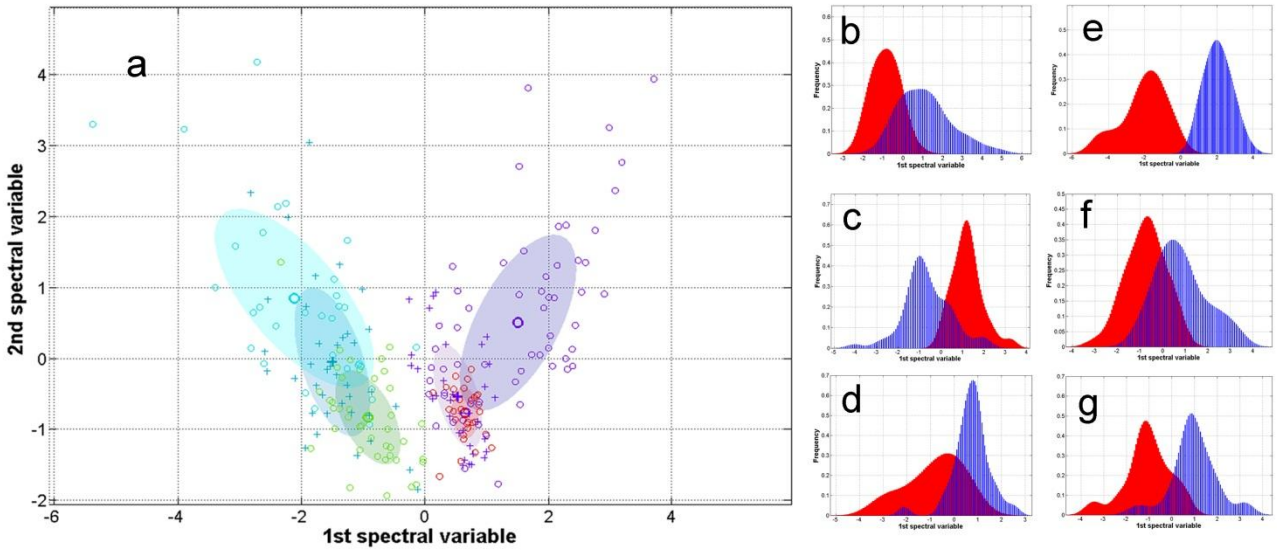

Fig. 1. Healthy, 11% and 44% MELAS and 11% and 44% MELAS treated cells form statistically separate clusters with respect to autofluorescence properties. a) Scatterplot of average cell spectra in optimised spectral space. Symbols represent average cell spectra for each cell, the colour of these small symbols identifies patients. Green circles: healthy control cells for 11%, red crosses: healthy controls for 44%; cyan circles: 11%, blue crosses: 11% treated; blue circles: 44%; blue crosses: 44% treated cells. Large symbols- mean values for each cell classes, ovals - regions within the single standard deviation from the b-g) histograms (Parzen estimates, see Sup. Mat. S4*) of the selected pairs of cell classes. Numbers in brackets give statistical distance. b) 11%- blue, healthy-red (**1.87**); c) 44%-blue, healthy-red (**1.98**); d) 11% -blue, 11% treated-red (1.05); c) 44%-blue, 44% treated-red (**8.89**); d) 11%treated-blue, healthy-red (*1.17*); e) 44% treated-blue, healthy-red (**1.42**).*

Clear separation of clusters in Fig. 1 a confirms that the cells from MELAS patients can be distinguished from healthy cells. Moreover, cells from two different patients also form different clusters, thus all three cell classes are well separated. To statistically analyse the cluster separations, we carried out a second LDA projection of our data. For this new projection, two classes of cells were chosen at a time, and their average spectra were projected onto a common line. This approach visualises cell distributions by histograms (Fig. 1 b, c) and provides statistical distance (Sup.Table 1). The Kolmogorov-Smirnov test of the hypothesis that every two classes selected among all three (healthy, MELAS, treated) come from the same distribution gave *p*-values of less than 10^{-12}, consistently with Fig. 1 a.

The analysis of the cells that have undergone galactose treatment to reduce the mutational load is shown in Fig. 1 a. The treated cell group moves away from MELAS cells and noticeably approach the healthy cells region. Pairwise LDA projections produced histograms shown in Fig 1 d-g which are also well separated (See Sup. Table 1 for statistical distances). Overall, our results indicate that cells exposed to galactose are brought closer to healthy control cells compared to MELAS cells. Thus our method can not only distinguish MELAS on a cellular level but also quantify the response of such cells to pharmacological interventions.

Mapping of key fluorophores in cells

In order to shed light on cell biochemistry we decomposed the spectral images of the cells under investigation into five most significant spectral components representing the most prominent fluorophore groups. This analysis uses an unsupervised unmixing approach (see Methods). The resulting component (endmember) spectra are shown in Fig. 2 a-e (44% MELAS) and Sup. Fig. S1 a-e (11% MELAS) where they are found to correspond to the spectra of bound flavin, FAD, A2E, bound NADH, free NADH, flavins and lipofuscin, the most abundant cellular fluorophores according to the literature [15]. All groups of cells had significant contributions of free and bound NADH as well as A2E and lipofuscin. The fifth spectral component was different in the two examined cases: FAD in 11% MELAS (and 11% treated and control cells) and bound flavins in 44% MELAS (and 44% MELAS treated and controls).

To lend further support to our assignment we carried out colocalisation analysis of autofluorescence endmembers with organelle stained images. (Sup. Figs S2, S3, S4). Here, an adaptive algorithm has been used to correct for the cell motion. The image correlations between the endmembers and individual stains are displayed in Sup. Fig. S4. We confirmed (a) high degree of colocalisation between flavins and stained mitochondria; (b) the absence of colocalisation between free NADH bound NADH (correlation of 0.17); (c) strong colocalisation of bound NADH and the mitochondria, with correlation values r between 0.62 and 0.9); and (d) co-localisation of retinoids with the liposomes and the mitochondria.

Finally, we checked that that the fluorescence of the identified fluorophores appropriately responds to chemical quenching. To this aim we applied several known fluorescence quenchers including (a) sodium borohydride which reduces free NAD^+ to fluorescent NADH and reduces fluorescent flavins thus quenching their fluorescence; (b) acrylamide which quenches flavins;(c) FCCP [33] and rotenone [34] (specific to NADH) and confirmed their quenching effect on the fluorescence intensity (see Sup. Fig. S5).

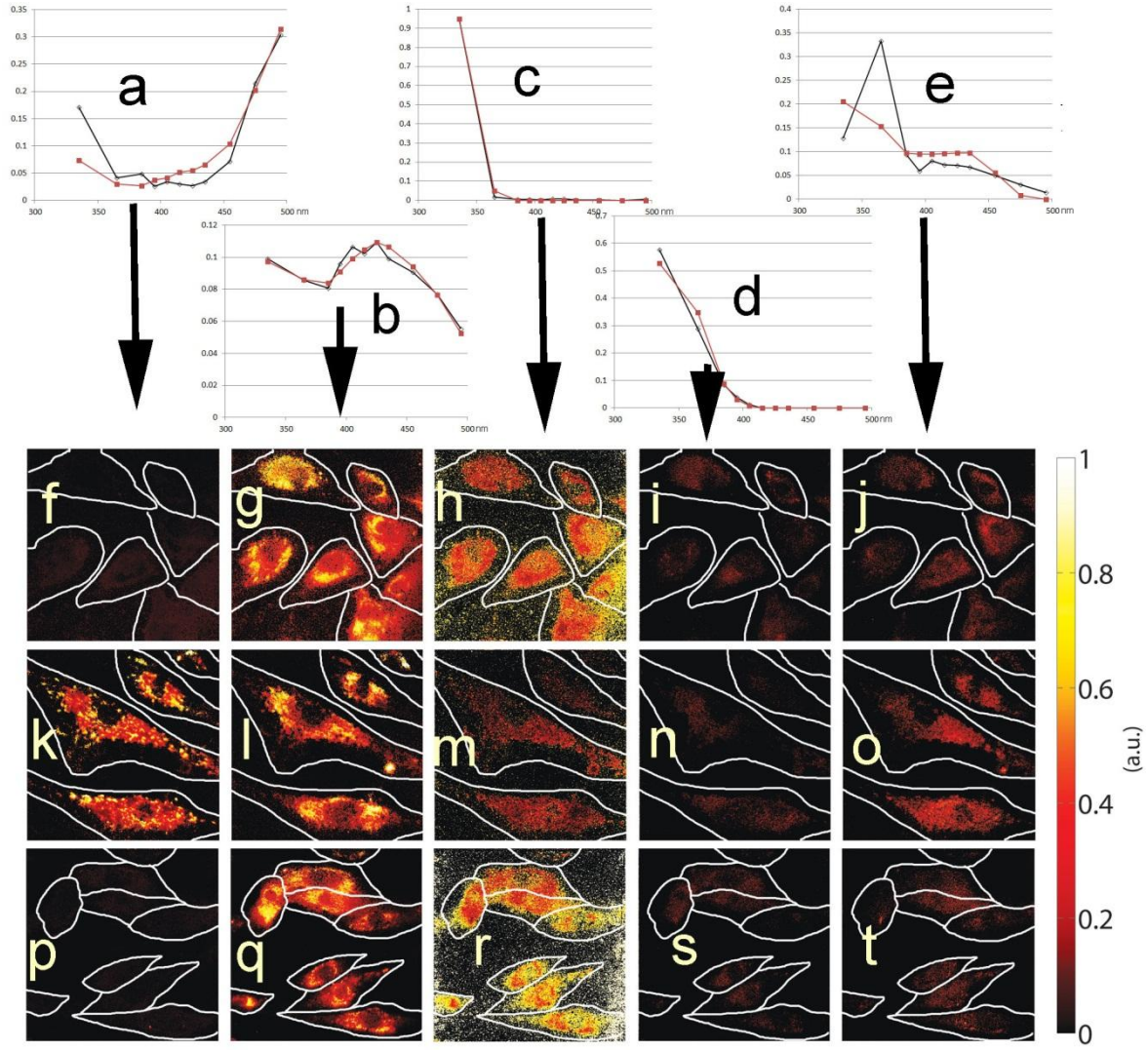

Fig.2 a-e: Comparison of the spectra of five key fluorophores (red) in 44% MELAS cells with endmembers identified in our images by unsupervised unmixing (black). Our endmembers agree well with (a) bound flavins, (b) A2E, (c) bound NADH, (d) free NADH and (e) lipofuscin. Below we show images of cells showing the abundance of the five key fluorophores in healthy control (top row: f-j), 44% MELAS (middle row: k-o) and 44% MELAS treated patient (bottom row: p-t). Columns from left to right: f,k,p – bound flavins; g,l,q- A2E; h,m,r- bound NADH; i,n,s -free NADH; j,o,t - lipofuscin. The outlines of cells have been marked for clarity. The colour scale reflects fluorophore abundance.

Our approach produced cellular maps of each of the five key fluorophore groups within the examined cells. These are shown in Fig. 2 f-t where we present the results for the 44% MELAS patient before and after galactose treatment and the controls (see Sup. Fig. S1 f-t for 11% MELAS). The average cell intensities in Fig. 2 f-t show clear trends, also statistically confirmed in all cells by boxplots (Sup. Fig. S6). For example, the flavin content is low in healthy cells, high in 44% MELAS and it returns to almost healthy levels after treatment. The bound NADH content is high in healthy cells, low in MELAS and it increases after treatment, while the opposite is true for free NADH. The fluorescence levels of retinoids are higher in healthy and MELAS treated cells, but lower in MELAS cells. Sup. Fig. S1 f shows that flavins in healthy cells are mostly located outside of the nuclear region. In MELAS cells (Fig. 2 k and Sup. Fig. S1 k) they are highly concentrated in

filamentous structures surrounding the nucleus and they are also found in the nucleus, but with a smaller density. The galactose treatment brings down the average flavins contribution and they can be seen mostly outside of the nucleus, similarly to the "healthy" distribution (Sup. Fig. S1 p). Bound NADH is comparatively less abundant in MELAS than in healthy cells (Fig. 2 h, m and Fig. S 1 h, m) and it is absent in the nuclear region of MELAS cells. Retinoids in healthy cells (Fig. 2 g,j) and Fig. S1 g,j) form perinuclear rings consistent with their mitochondrial localisation [14, 35] with some contribution from the lysosomes as well. Our colocalisation analysis of different endmembers was also consistent with the assignment of the fluorophore groups observed in this study (see Sup. Fig. S7 and Supplementary Discussion).

Metabolic imaging

Further, we obtained the optical redox ratio, defined as the ratio of fluorescence signals from flavins to flavins and/or NAD(P)H extensively used in the literature as a measure of the oxidation/reduction status in a cell which is sensitive (inversely related) to the cellular metabolic rate [11, 12, 36, 37]. This approach is based on the observation that mitochondrially localized NAD(P)H [34, 35] and flavins (LipDH and ETF) are directly linked to cellular metabolic activity. [38].

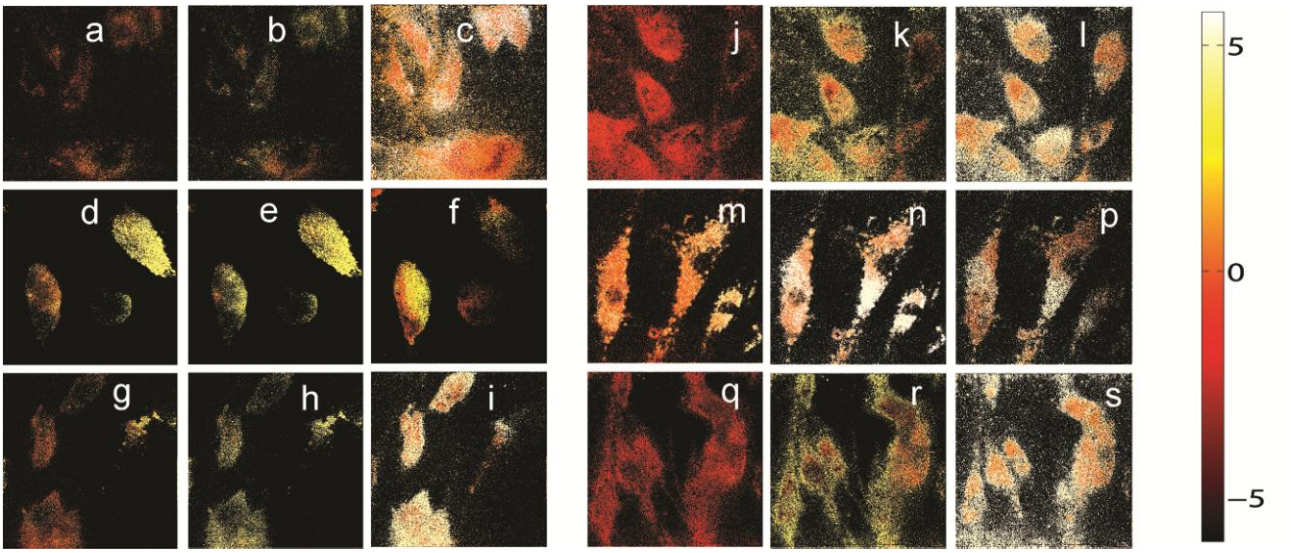

Fig. 3. Metabolic imaging of cells. The end member abundance images are divided to produce ratio images. All values undergo the log (base 2) transform (see colour scale). Left panel (a-i) – 11% MELAS, right panel: (j-s) – 44% MELAS. Top row: healthy, middle row: MELAS, bottom row: MELAS treated. (a,d,g) – ratio of FAD to bound NADH. (b,e,h): ratio of FAD to free NADH, (c,f,i): ratio of bound to free NADH, a measure of balance between glycolysis vs oxidative phosphorylation; (j,m,q): ratio of flavins to bound NADH. (k,n,r): ratio of flavins to free NADH, (l,p,s): ratio of bound to free NADH.

The optical redox ratios in the examined cells are presented in Fig. 3. We show that MELAS cells have a much higher optical redox ratio than the control healthy cells, consistent with their impaired metabolic activity which is largely, but not completely restored by the galactose treatment. We also present the cell images displaying the ratio of bound to free NADH (Fig 3 c, f, i, l, p, s). These confirm that the MELAS cells show lower levels of bound/free NADH (hence enhanced glycolysis) compared with the normal cells where the bound NADH signal from oxidative phosphorylation is stronger. A more detailed statistical analysis for the whole ensemble of cells within the sequence healthy-MELAS-MELAS treated is shown in Sup. Fig. S6 confirming similar trends.

Identification of cell subpopulations

We used our automated algorithm described in Methods to search for cell subpopulations by looking for clustering of fluorophore abundances illustrated in Fig. 4 a-r with statistical analysis before and after galactose treatment shown in Sup. Fig. S8.

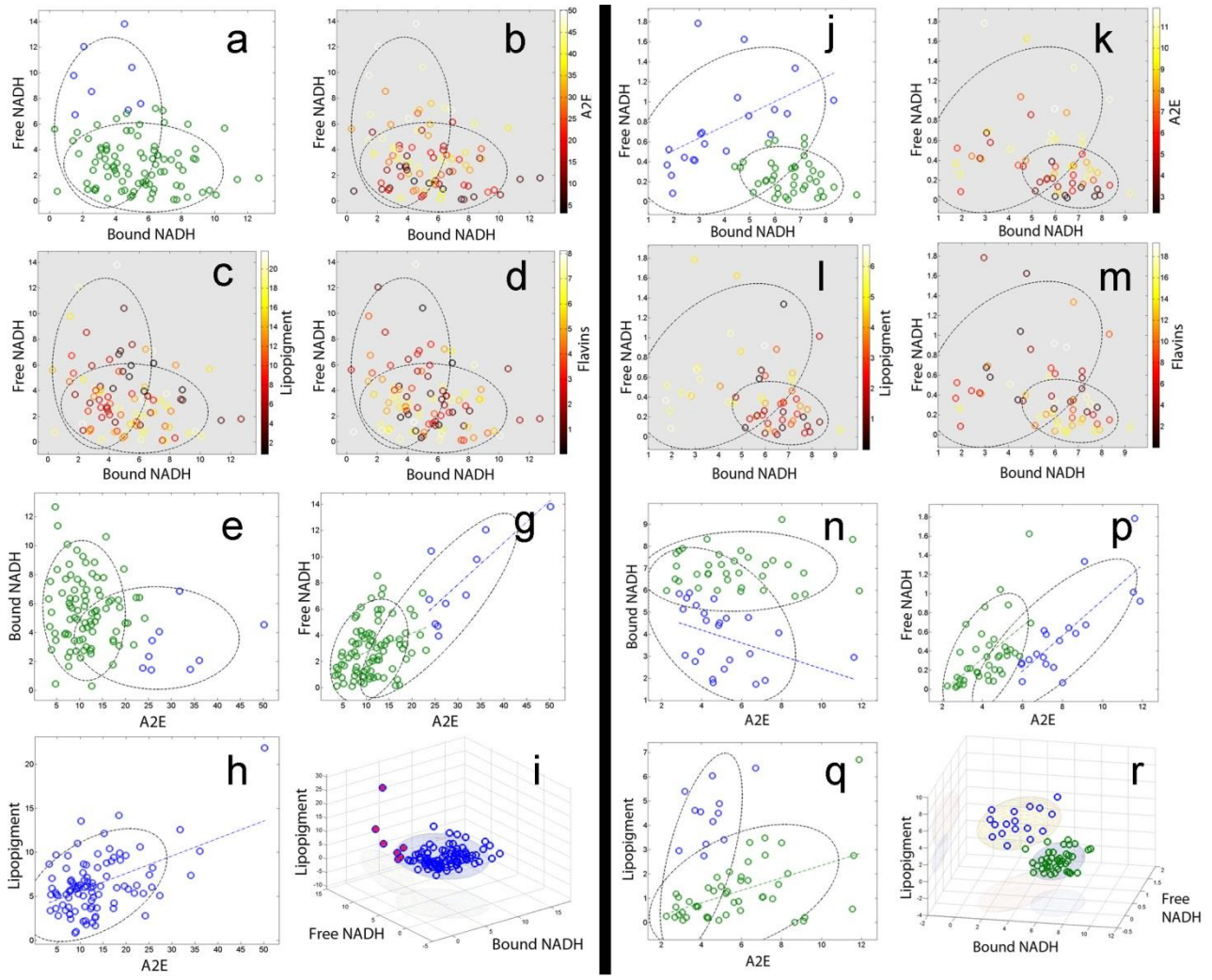

Fig. 4. Scatterplots showing the most pronounced correlations between fluorophore abundances in cells and cell subpopulations (a-i) 11% MELAS,(j-r)- 44% MELAS. Fluorophores are indicated on the axes. The colour scale in plots with grey background indicates the abundance of the third fluorophore. All plots presented here have the best mixture model value which is greater than unity.

In order to obtain the plots shown here, all combinations of features have been tested and scored in terms of how well they clustered into any of the shaded regions, indicating subpopulation coincidence. This was done for all features shown to have definite 1D sub populations. Such multidimensional analysis provides a more detailed view of sub-populations and it makes it possible to detect new sub-populations showing covariances which otherwise could remain hidden. In particular we draw attention to completely separated and almost even two subpopulations in Fig 4 r for 44% MELAS (green and blue) and two uneven well-separated subpopulations (red and blue) for 11% MELAS (Fig. 4 i). We also draw attention to the behaviour of the optical redox ratio (flavins: bound NADH, (Sup. Fig. S8) showing clear subpopulations in the MELAS patients. These

subpopulations later disappear after galactose treatment. The ratio of free NADH/bound NADH which is a relative measure of glycolysis and several other features also show clear subpopulations (Sup. Fig. S8).

Comparison with biochemical characterisation

Sup. Fig. S9 summarises the results of biochemical characterisation of the examined cell groups. It shows that the biochemistry of MELAS cells is significantly altered compared to healthy controls. For example the ATP production and MTMP are clearly lower than healthy, while the levels of lactate and SOX are clearly elevated. These values return closer to healthy levels after treatment.

Discussion

Originally developed for remote sensing, this work expands the hyperspectral approach to the fields of medicine and cell biology in areas utilising fluorescence microscopy. It yields quantitative and straightforward interpretation of physiological processes in living tissues similar to multiphoton fluorescence and/or FLIM but without the complexity and cost of a multiphoton FLIM imaging system. The use of single photon fluorescence at comparatively low excitation irradiances (in the order of 10^3 W/cm^2) from light emitting diodes is also an advantage. We have shown here that the hyperspectral approach combined with high content data mining of cell images provides novel insights into the MELAS disease which is characterised by genetically determined mitochondrial dysfunction. Olfactory neurosphere cells investigated here are disease–specific models of neuronal disorders [1], thus our work offers new ways of understanding these and a broad range of other diseases affecting metabolism.

By using our hyperspectral analysis to differentiate cell groups we were able to statistically establish that MELAS cells differ from healthy cells, confirming high sensitivity of the method (Fig. 1); such certainty is impossible to gain from the biochemistry data alone for these patients. Even more importantly, we have been able to distinguish cells from each MELAS patient before and after treatment and demonstrate that they are now more similar to the healthy cells than before treatment. The method produces *p*-values for the hypothesis that the two cell groups are different. Our method is also robust with respect to reproducibility and the same results have been obtained in repetitive cell experiments from different cell passages four months apart period. These results show that hyperspectral analysis is sensitive enough to monitor functional treatment response of cells from single individuals.

Unlike in other works ([14]) our spectra have sufficient spectral resolution to differentiate between unbound and protein-bound forms of NADH, whose spectrum is blue-shifted by 20 nm compared to free NADH [39, 40]. However we are unable to differentiate between NADH and NADPH, thus the NADH components in this work (free or bound) represents both NADH and NADPH fluorescence [26]. The flavins component represents the majority of the cellular flavins fluorescence produced by the mitochondrial lipoamide dehydrogenase (LipDH) and electron transfer flavoprotein (ETF), but also flavins generated in cytosol. The shape of the flavins excitation spectrum is similar to that of aqueous flavins with a red shift by 50 nm by the effect of protein binding [33,41-43]. We have been able to separately identify FAD [14]. In the retinoid group, the A2E has also been separately identified, while the spectrally similar retinoids [44,45] including retinol, retinoic acid as well as

cellular retinol-binding proteins (CRBPs) and cellular retinoic acid-binding proteins (CRABPs) which carry retinoids within cells have been merged with lipofuscin.

We also carried out a detailed colocalisation analysis (Sup. Fig. S7) of the fluorescent components presented in Fig. 2 and Sup. Fig. S1. In order to validate our assignments we only focussed on healthy cells (Sup. Fig. S7). We found that (a) free and bound NADH do not colocalise, in agreement with their cellular localisation in the mitochondria and cytosol, respectively; (b) flavins colocalise with bound NADH; this is because they are both localised in the mitochondria, however there are also uncolocalised cytosolic flavins as expected [46]; (c) lipofuscin located in the lysosomes does not colocalise with bound NADH in the mitochondria. All these colocalisations are in agreement with the established knowledge about the behaviour of these fluorophore groups in cells. In Supplementary Discussion we analyse trends in fluorophore content and their ratios between healthy, MELAS and treated cells in comparison with traditional biochemistry.

Our results indicate that the cells in the 44% mutant MELAS cells show a comparatively lower level of metabolic activity than the control and that the redox ratio is restored to the near-healthy level by galactose treatment. This is consistent with our biochemistry results which show that ATP production was reduced in MELAS compared to both healthy and MELAS treated cells (Fig. S9). We also found that the free to bound NADH ratio varied significantly; it was low in healthy controls, increased considerably in MELAS but it returned back to almost normal after galactose treatment (Sup. Fig. S6 b). The ratio of bound to free NADH has biological significance, because oxidative phosphorylation in the mitochondria predominantly (in 80%) produces protein-bound NADH [21, 47] while glycolysis produces free NADH in the cytosol [48]. Thus the ratio of bound to free NADH reflects the balance between glycolysis and oxidative phosphorylation. The inspection of Sup. Fig. S6 b indicates that in 44% MELAS cells the bound to free NADH ratio was lower than in the matched control. Such increased glycolysis and/or decreased oxidative phosphorylation in MELAS cells compared to healthy controls is indicative of the switch of the higher mutant MELAS cells to alternative bioenergetic pathways to supply ATP in the absence of sufficient oxidative phosphorylation, even though glycolysis produces less ATP from the same amount of glucose. This is also demonstrated by the apparent increased lactic acid, a by-product of glycolysis but not of oxidative phosphorylation (Sup. Fig. S9). Overall, our results indicate that hyperspectral imaging reflects the metabolic function in vivo in individual cells, and it can detect metabolic activity through the optical redox ratio and the balance of glycolysis and oxidative phosphorylation. We have shown that it can help assess the disease status and the effect of therapies in olfactory neuronal cells, which serve as models for a variety of neurodegenerative diseases. Using this method it will be possible to analyse impairment of the metabolic function in these diseases as well as monitor neuronal activity in vivo [27] once the ONS cells are differentiated into functioning neurons.

The existence of cell subpopulations with respect to the identified fluorophore groups is shown in Sup. Fig. S8. For example we observe that healthy cells display a single population only with respect to flavins content, while 44% MELAS cells show two distinctive and separate subpopulations. After galactose treatment the average flavins level decreases but the two subpopulations are still apparent. The subpopulations are also clearly pronounced for both bound and free NADH and this may be related to progress some of the cells have inadvertently made along the differentiation pathways; we have independently checked that hyperspectral imaging is indeed capable to detect such early differentiation in stem cells. Finally, our healthy cells constituted a

single population with respect to the retinoids' content, but clear subpopulations are observed in MELAS and MELAS treated cells. Sup. Fig. S8 shows a similar analysis for fluorophore ratios, again displaying clear subpopulations in most cases. These subpopulations are particularly pronounced in MELAS cells for flavins to bound NADH and retinoids to bound NADH ratios. These subpopulations are associated with varying levels of metabolic activity and glycolysis.

Specific subpopulations visualised in Fig. 4 and Sup. Fig. S8 are analysed in Supplementary Discussion. These results indicate that MELAS cells in this patient belong to two distinctive classes, which we tentatively identify as "healthy" (green) and "mutated" (blue). Thus our data support the hypothesis that MELAS is a disease which affects cells to a different degree as opposed to the alternative that all cells are similar and characterised by a certain proportion of defective mitochondria in each. Distinguishing between these two hypotheses is significant for the design of patients' treatment regimens.

METHODS (ONLINE)

Details of biological experiments

In this study we used cells from the MELAS patient-derived olfactory-derived neurospheres (ONS) with varying levels of mutational load (11% and 44%) generated from olfactory primary cultures. To prepare these ONS, nasal biopsies were carried out and harvested cells were expanded and subcultured as described in more details in Sup. Mat. S1. Cells from healthy control subjects were harvested and treated in the same fashion. The MELAS cells were subjected to galactose-supplemented, glucose-free media (starvation) over a period of 4 days. We present data from three different cell passages. Imaging was carried out on cells having an approximately constant cell density. Each cell sample was prepared and imaged in duplicate. Altogether, over 1500 cells were imaged in this study.

Cells were carefully characterised biologically by a variety of methods. In particular we measured mutational load by standard radiolabelled ("hot-finish") PCR/RFLP analysis, carried out the citrate synthase assay for the determination of mitochondrial mass, measured the level of lactate, ATP, mitochondrial superoxide generation (SOX), mitochondrial transmembrane potential by flow cytometry. All cells were also imaged by laser scanning microscopy, with Green Mitotracker, Red Lysotracker and Blue Er-Tracker staining. (see Sup. Mat. S2 for more details)

Hyperspectral measurements technique

Our method uses fluorescence of native fluorophores commonly found in cells. In our approach the images of live cells are obtained by an Andor IXON camera under illumination at a number of selected bands of excitation wavelengths (here, centred at 334, 365, 385, 395, 405, 415, 425, 435, 455, 475, 495 nm, each about 10 nm wide). The emission is measured in the range 550 nm- 600 nm. These measurements yield fluorescence excitation spectra measured at each pixel for all images of cells coming from all patients. These spectra are further corrected for instrumental response. A "background" reference image of a culture dish with a medium is also taken and subtracted from all images with cells.

Description of data analysis method for differentiation of cell groups:

The original pixel spectra containing intensity and wavelength information are represented as vectors in an n-dimensional spectral space whose coordinates are intensities at each of the n excitation wavelength (here, n=11). This dataset contains significant correlations, as cell images at adjacent wavelengths are very similar; this is first removed by using a covariance matrix calculated from the data. (see Sup. Mat. S4 for mathematical details). Further, we calculate average cell spectra. The method of Linear Discriminant Analysis (LDA) [49] is then employed, in order to establish whether these average spectra from biologically identifiable classes of cells form well separated clusters. In this method we first choose the m cell classes and by using LDA we project the original n-dimensional spectral space and the data points representing the average spectra of our cells onto a new, lower-dimensional space. Its dimension is given by the number of groups of cells classes to be distinguished less 1. For convenience of presentation, in this work we have been using three classes of cells, so that after LDA the spectra of these cells can be depicted as points on two dimensional plots. This two-dimensional spectral space produced by LDA is referred to as the "canonical spectral space". Its basis vectors are orthogonal, and aligned with the axes in our relevant figures.

The LDA method ensures that the new space is optimised to provide the best degree of separation between selected cell classes (such as, for example, cells from different patients). Finally, to quantify the distinctiveness between selected pairs of cell clusters we perform the LDA analysis again, on each pair of cell cluster data projecting them onto a one-dimensional line. The Kolmogorov-Smirnov statistical test is then applied to gauge and compare the similarity of the pair of clusters. We also calculate the maximum Fisher statistical distance, a measure of cluster closeness which is sensitive to cluster means and takes account of the data dispersion.

We add that the data for additional cells and/or patients or data produced by other authors may be plotted together with our data. Although there is no mathematical certainty that optimum separation will be achieved for such blended datasets, a clear separation may often be achieved in the case when class distinction results are statistically strong with small *p*-values.

Description of data analysis method to determine fluorophore abundance

We are assuming that the observed spectra are a linear combination of fundamental spectra originating from particular substances, called end members. These N number of endmember spectra X are weighted by an abundance coefficient vector f such that an observed spectrum $\mathrm{Z_p}$ which is given by equation (1):

$$Z_p = Xf + e = \sum_{i=1}^{N} X_i f_i + e \qquad (1)$$

where e is the residual, or noise, not explained by the mixture of end members.

The problem of finding the endmembers has a simple geometrical interpretation. The spectra of all individual pixels in cells represent a certain cluster in an N dimensional space. The cluster is contained within a convex hull called a simplex and each pixel spectrum point within this simplex represent a linear combination of the spectra represented by the extreme points (vertices) of that simplex. These vertex spectra are chosen to be end members.

In order to find the best simplex representing the data points two conditions need to be satisfied: that the coefficients of the abundance vector are all positive and that they add up to unity. To

identify that best simplex we minimised the least squares error between the targets spectra and the product of our abundance vector multiplied by the end member spectra, for the entire set of data.. The corresponding endmembers spectra are shown in Fig. 2 and Sup. Fig. S1. Fit errors are typically being between 5-10%, due to the presence of other less abundant and unidentified residue spectra.

Description of data analysis method to detect cell subpopulations

In order to characterise subpopulations in the examined cells we first specify *K*, the number of subpopulations we wish to find in each data group (*K=2* in the presented analysis). Then for all groups within all variables, the data undergo an unsupervised mixture model. The non-deterministic algorithm is used to break the data into potential subpopulations. Each produced solution goes through selection criteria so that only the highest scoring solution per data group is selected. The criteria are that each of the subpopulations must be > 30% of the whole dataset, the subpopulations must have a statistical separation greater than, 1 and they must pass a Kolomogorov-Smirnov test with $P<0.05$. The mixture model returns only the subpopulation means and covariance, so in order to classify the data points in one of the K subpopulations we used a Naive Bayes classifier. The method reproducibly finds subpopulations that agree with intuition when looking at the histograms. Boxplots are used to give an overview of data and a visualisation has been created to display groups of data with subpopulations. The width of the subpopulation boxes is proportional to their size, to allow some inference power across groups.

References

1. Matigian, N.*et al* .Disease-specific, neurosphere-derived cells as models for brain disorders. *Dis. Model. Mech*. **3**,785-98(2010).

2. Wolozin, B. *et al*. Continuous culture of neuronal cells from adult human olfactory epithelium. *J Mol. Neurosci*. **3**(3) , 137-46(1992).

3. Abrams, M.T. *et al*. FMR1 gene expression in olfactory neuroblasts from two males with fragile X syndrome. *Am. J. Med .Genet*. **82**(1), 25-30(1999).

4. Feron, F., Perry, C., Hirning, M.H., McGrath, J.& Mackay-Sim, A. Altered adhesion, proliferation and death in neural cultures from adults with schizophrenia. *Schizophr. Res*. **40**(3), 211-8(1999).

5. Arnold, S.E. *et al*. Dysregulation of olfactory receptor neuron lineage in schizophrenia. *Arch. Gen. Psychiatry*. **58**(9), 829-35(2001).

6. Ronnett, G.V. *et al*. Olfactory biopsies demonstrate a defect in neuronal development in Rett's syndrome. *Ann. Neurol*. **54**(2), 206-18(2003).

7. McCurdy, R.D. *et al*. Cell cycle alterations in biopsied olfactory neuroepithelium in schizophrenia and bipolar I disorder using cell culture and gene expression analyses. *Schizophr. Res*. **82**(2-3), 163-73(2006).

8. Haehner, A. *et al*. Prevalence of smell loss in Parkinson's disease--a multicenter study. *Parkinsonism. Relat .Disord*. **15**(7), 490-4(2009).

9. Chance, B., Williamson, J. R., Jamieson, D. & Schoener,B. Properties and kinetics of reduced pyridine nucleotide fluorescence of the isolated and in vivo rat heart. *Biochem. Z*. **341**,357-377(1961).

10. Skala, M.C. *et al*. Multiphoton microscopy of endogenous fluorescence differentiates normal, precancerous, and cancerous squamous epithelial tissues. *Cancer. Res*. **65**, 1180-6(2005).

11.Skala, M.C. *et al*. In vivo multiphoton fluorescence lifetime imaging of protein-bound and free nicotinamide adenine dinucleotide in normal and precancerous epithelia. *J Biomed. Opt*. **12**(2), 024014(2007).

12. Skala, M.C. et al. In vivo multiphoton microscopy of NADH and FAD redox states, fluorescence lifetimes, and cellular morphology in precancerous epithelia. *Proc. Natl. Acad. Sci* ,U S A. 2007. **104**(49),19494-9(2007).
13.Uchugonova, A. & Konig,K. Two-photon autofluorescence and second-harmonic imaging of adult stem cells. *J Biomed. Opt*, 2008. **13**(5), 054068(2008).
14. William L. R., David L. K.& Irene G. Two-photon microscopy for non-invasive, quantitative monitoring of stem cell differentiation. *PLoS One*.**5**, 10075(2010).
15. Stringari, C. *et al*. Phasor approach to fluorescence lifetime microscopy distinguishes different metabolic states of germ cells in a live tissue. *Proc. Natl. Acad. Sci,USA* . **108**(33),13582-7(2011).
16. Stringari, C. *et al*., Metabolic trajectory of cellular differentiation in small intestine by Phasor Fluorescence Lifetime Microscopy of NADH. *Sci Rep*.**2**,568(2012).
17 Stringari,C., Jamison, L., Lisa, N., Flanagan,A.& Grattone,E. Phasor fluorescence lifetime microscopy of free and protein-bound NADH reveals neural stem cell differentiation potential. *PLoS One*.**7**(11),48014(2012).
18. Stringari, C., Sierra, R., Donovan, P.J.& Gratton, E .Label-free separation of human embryonic stem cells and their differentiating progenies by phasor fluorescence lifetime microscopy. *J Biomed Opt*.**17**(4),046012(2012).
19.Wright, B.K. *et al*. Phasor-FLIM analysis of NADH distribution and localization in the nucleus of live progenitor myoblast cells. *Microsc. Res. Tech*. **75**(12), 1717-22(2012).
20.Wright, B.K. *et al*. NADH distribution in live progenitor stem cells by phasor-fluorescence lifetime image microscopy. *Biophys J*. **103**(1), L7-L9(2012).
21.Zipfel, W.R. *et al*. Live tissue intrinsic emission microscopy using multiphoton-excited native fluorescence and second harmonic generation. Proc *Natl. Acad. Sci, U S A*. **100**(12),7075-80(2003).
22.Rodrigues, R.M., Macko, P., Palosaari,T.& Whelan MP. Autofluorescence microscopy: a non-destructive tool to monitor mitochondrial toxicity. *Toxicol Lett*. **206**(3), 281-8(2011).
23.Field, M.G. Yang, D., Bian, Z.M., Petty, H.R.& Elner, V.M.Retinal flavoprotein fluorescence correlates with mitochondrial stress, apoptosis, and chemokine expression. *Exp Eye Res*. **93**(4), 548-55(2011).
24.Orzekowsky-Schroeder, R. *et al*. In vivo spectral imaging of different cell types in the small intestine by two-photon excited autofluorescence. *J Biomed. Opt*. **16**(11), 116025(2011).
25.Reinert, K.C. *et al*.Cellular and metabolic origins of flavoprotein autofluorescence in the cerebellar cortex in vivo. *Cerebellum*.**10**(3),585-99(2011).
26.Huang, S., Heikal, A.A. & Webb, W.W. Two-photon fluorescence spectroscopy and microscopy of NAD(P)H and flavoprotein. *Biophys J*, 2002. **82**(5) 28,11-25(2002).
27.Kasischke, K.A., Vishwasrao, H.D., Fisher,P.J., Zipfel, W.R.& Webb, W.W. Neural activity triggers neuronal oxidative metabolism followed by astrocytic glycolysis. *Science*. **305**(5680), 99-103(2004).
28.Chomyn, A. *et al*. MELAS mutation in mtDNA binding site for transcription termination factor causes defects in protein synthesis and in respiration but no change in levels of upstream and downstream mature transcripts. *Proc. Natl. Acad. Sci, U S A*. **89**(10),4221-5(1992).
29.Cotan, D.*et al*. Secondary coenzyme Q10 deficiency triggers mitochondria degradation by mitophagy in MELAS fibroblasts. *FASEB J*. **25**(8),2669-87(2011).
30.Sproule, D.M. & Kaufmann,P. Mitochondrial encephalopathy, lactic acidosis, and strokelike episodes: basic concepts, clinical phenotype, and therapeutic management of MELAS syndrome. *Ann N Y Acad Sci*. **1142**,133-58(2008).
31.de Andrade, P.B. et al. Diabetes-associated mitochondrial DNA mutation A3243G impairs cellular metabolic pathways necessary for beta cell function. *Diabetologia*. **49**(8),1816-26(2006).
32.Shepherd,R.K.*et al*. Measurement of ATP production in mitochondrial disorders. *J Inherit Metab Dis*. **29**,86-91(2006).
33.Chapman, S.K. Flavoprotein Protocols. *Methods in Molecular Biology*. (Humana Press , New Jersy,1999).

34.Frezza, C. *et al*.Metabolic profiling of hypoxic cells revealed a catabolic signature required for cell survival. *PLoS One*. **6**(9),24411(2011).
35.Ruff, S.J. & Ong,D.E. Cellular retinoic acid binding protein is associated with mitochondria. *FEBS Lett*. **487**(2),282-6(2001).
36.Kirkpatrick, N.D. *et al*. Endogenous fluorescence spectroscopy of cell suspensions for chemopreventive drug monitoring. *Photochem Photobiol*. **81**(1),125-34(2005).
37.Shiino, A., Haida, M., Beauvoit, B., Chance, B. Three-dimensional redox image of the normal gerbil brain. *Neuroscience*. **91**(4), 1581-5(1999).
38.Chance, B., Schoener, B., Oshino, R., Itshak, F.& Nakase, Y. Oxidation-reduction ratio studies of mitochondria in freeze-trapped samples. NADH and flavoprotein fluorescence signals. *J Biol. Chem*. **254**(11),4764-71(1979).
39.Chance, B. & Baltscheffsky,M. Spectroscopic effects of adenosine diphosphate upon the respiratory pigments of rat-heart-muscle sarcosomes. *Biochem J*. **68**(2),283-95(1958).
40.Piersma, S.R., Visser, A.J., de Vries, S., Duine, J.A., Optical spectroscopy of nicotinoprotein alcohol dehydrogenase from Amycolatopsis methanolica: a comparison with horse liver alcohol dehydrogenase and UDP-galactose epimerase. *Biochemistry*. **37**(9),3068-77(1998).
41.Lakowicz, J., *Principles of fluorescent spectroscopy* .3rd Edition. (Springer, 2006).
42.Fjeld, C.C., Birdsong, W.T.& Goodman, R.H. Differential binding of NAD_ and NADH allows the transcriptional co-repressor carboxyl-terminal binding protein to serve as a metabolic sensor. . *Proc. Natl. Acad. Sci, U S A*. **100**(16), 9202-7 (2003).
43.Kasimova, M.R.*et al*. The Free NADH Concentration Is Kept Constant in Plant Mitochondria under Different Metabolic Conditions. *The Plant Cell*. **18**(3), 688–98(2006).
44.Gundersen, T.E. Methods for detecting and identifying retinoids in tissue. *J Neurobiol*. **66**(7),631-44(2006).
45.Haralampus-Grynaviski, N.M. *et al*. Spectroscopic and morphological studies of human retinal lipofuscin granules. *Proc. Nat.. Acad. Sci, U S A*. 2003. **100**(6),3179-84(2003).
46.Tu, B.P. &Weissman, J.S. The FAD- and O(2)-dependent reaction cycle of Ero1-mediated oxidative protein folding in the endoplasmic reticulum. *Mol Cell*. **10**(5),983-94(2002).
47.Blinova, K.*et al*. Distribution of mitochondrial NADH fluorescence lifetimes: steady-state kinetics of matrix NADH interactions. *Biochemistry*, 2005. **44**(7),2585–94(2005).
48.Overkamp, K.M.*et al*. In vivo analysis of the mechanisms for oxidation of cytosolic NADH by Saccharomyces cerevisiae mitochondria. *J. Bacteriol*. **182**(10),2823-30(2000).
49.Jieping, Y. Characterisation of a family of algorithms for generalized discriminant analysis on under sampled problems. *Journal of Machine Learning Research*. **6**,483-502(2005).

Acknowledgements

This work was partially supported by the Australian Research Council (ARC) through its Centre of Excellence scheme (CE140100003).

Contributions

E.G., C.S. and M.G. designed the experiments. M.G., J.C.and A.A. performed the experiments. M.G and E.G. analyzed the data. E.G.,C.S., M.G., J.C. and A.A. wrote the manuscript. All authors have reviewed the manuscript.

Competing financial interests

Dr Martin Gosnell runs a bioinformatics data analysis company and has an interest in developing similar technologies and applications. Other authors have no competing financial interests.